ELSEVIER

Polymer 43 (2002) 4869–4877

polymer

www.elsevier.com/locate/polymer

Coupling of mutual diffusion to viscoelasticity in moderately concentrated polyisobutylene solutions

Yoshiyuki Einaga[a,*], Ayako Itaya[a], Motoki Takaoka[b]

[a]*Department of Chemistry, Nara Women's University, Nara 630-8506, Japan*
[b]*Department of Polymer Chemistry, Kyoto University, Kyoto 606-8501, Japan*

Received 8 February 2002; received in revised form 7 May 2002; accepted 27 May 2002

Abstract

The normalized intensity autocorrelation function $g^{(2)}(t)$ were obtained by dynamic light scattering for moderately concentrated entangled solutions of polyisobutylene in *n*-heptane at 25.0 °C and in isoamyl isovalerate (IAIV) at 25.0 °C (Θ). The obtained data have been successfully analyzed by the 'procedure X' familiar for determination of mechanical relaxation spectra on the basis of the recent theory for $g^{(2)}(t)$. The results have shown that while the mutual diffusion coefficient D increases in the *n*-heptane solutions and decreases in the IAIV solutions with increasing polymer mass concentration c, the friction coefficient ζ for both solutions increases with c showing the same power-law behavior irrespective of the weight-average molecular weight M_w and solvent quality. It has been found that the instantaneous longitudinal modulus L_0 for *n*-heptane solutions increases in proportion to c^2, obeying the familiar relation for the plateau value $(4/3)G_N$ of the longitudinal stress relaxation modulus, but L_0 for the IAIV solutions becomes progressively smaller than the values predicted from the relation with decreasing c. The terminal relaxation time τ_m has been found to follow the power-law $\tau_m \propto M_w^{3.4}$ established by rheological measurements.

Keywords: Dynamic light scattering; Viscoelasticity; Polyisobutylene

1. Introduction

Mutual diffusion in entangled polymer solutions is accompanied by viscoelastic relaxation since the diffusion of polymer and solvent molecules due to gradient of their chemical potentials induces disturbances of the equilibrium distributions of polymer chains. The coupling of diffusion to viscoelasticity is widely found in mass transport processes in polymer–solvent mixtures [1–3]. Concentration fluctuations in polymer solutions, from which light scattering results, are one of such processes. Thus, the dynamic structure factor $S(q,t)$, measured by dynamic light scattering (DLS) as a function of time t and the magnitude of scattering vector q, contains two contributions from the mutual diffusion and the viscoelastic relaxation processes.

Formulations of $S(q,t)$ have been given for these two decades by several authors [4–11], including one of the present authors, phenomenologically or in a molecular theoretical way. They have indicated that $S(q,t)$ is substantially composed of two terms which represent the so-called fast and slow modes in conformity with experimental observations [12–17]. It has been shown that both modes (or terms) include information on diffusional or frictional and viscoelastic properties of the polymer solution in a involved way depending on the value of q [6,9,11]. Thus, the DLS technique has been utilized to determine the relaxation times and their distributions for moderately concentrated polymer solutions to which conventional mechanical or rheological measurements are not readily accessible. Most of the data analyses of measured $S(q,t)$ have been, however, done so far by postulating that the slow mode is exclusively related to the viscoelastic relaxation and the fast one to the so-called cooperative diffusion process. The treatments are not always justified as mentioned previously [6,9,11].

In the previous paper [11], we have indicated a novel method to determine the rubbery plateau modulus and relaxation times of the entangled polymer solutions from $S(q,t)$ with some preliminary experimental results for polyisobutylene (PIB) solutions. The present paper reports more extensive results obtained from DLS measurements for moderately concentrated PIB solutions with good and Θ solvents. The purpose is twofold: one is to demonstrate how

* Corresponding author. Tel./fax: +81-742-20-3400.
E-mail address: einaga@cc.nara-wu.ac.jp (Y. Einaga).

0032-3861/01/$ - see front matter
PII: S0032-3861(02)00336-1

the mutual diffusion coefficient D, frictional coefficient ζ, longitudinal plateau modulus L_0, and terminal relaxation time τ_m are determined from the $S(q,t)$ data in a rather general way without resort to any specific molecular model. Another is to find dependencies of these physical properties on polymer molecular weight, concentration, and solvent quality.

2. Theoretical

For convenience, we briefly describe the basic equations required to analyze the experimental $S(q,t)$ data on the basis of our recent theoretical results [10,11] for $S(q,t)$ which is substantially equivalent to the one derived by Onuki [8] or Doi and Onuki [7]. The equation for concentration fluctuations in binary polymer solutions which contains the induced partial stress effect by the polymer chains yields the dynamic structure factor $\hat{S}(q,\omega)$ as a function of q and angular frequency ω as

$$\hat{S}(q,\omega) = \frac{1 + (1-\phi)\hat{L}(\omega)q^2/\mathrm{i}\omega c\zeta}{Dq^2 + \mathrm{i}\omega + (1-\phi)\hat{L}(\omega)q^2/c\zeta} \tag{1}$$

where ϕ is the polymer volume fraction, c the polymer mass concentration, and $\hat{L}(\omega)$ is the longitudinal dynamic modulus which is related to the longitudinal relaxation modulus $L(t)$ by

$$\hat{L}(\omega) = \mathrm{i}\omega \int_0^\infty \mathrm{e}^{-\mathrm{i}\omega t} L(t)\,\mathrm{d}t \tag{2}$$

$\hat{S}(q,\omega)$ is the Fourier transform of $S(q,t)$:

$$\hat{S}(q,\omega) = \int_0^\infty S(q,t)\,\mathrm{e}^{-\mathrm{i}\omega t}\,\mathrm{d}t \tag{3}$$

$L(t)$ is related to the compressional modulus $K(t)$ and the shear relaxation modulus $G(t)$ by [6,9,18]

$$L(t) = K(t) + \frac{4}{3}G(t) \tag{4}$$

For a polymer solution, as studied in this work, $K(t)$ and $G(t)$ may arise from the relaxation of fluctuations in the osmotic and shear moduli, respectively, as discussed by Berry [9] and Chen and Berry [6]. In this case, $K(t)$ is considered to be much smaller than $G(t)$ in magnitude and the relaxation time of $G(t)$ may be considerably larger than that of $K(t)$ if polymer concentration is large enough to produce entanglement effects [6]. The latter relaxation time is presumed to be very fast on the DLS time scale.

When the mechanical relaxation spectrum is approximated by an array of discrete line spectra, so that $L(t)$ is represented by

$$L(t) = \sum_{j=1}^{n} L_j\,\mathrm{e}^{-t/\tau_j} \tag{5}$$

$S(q,t)$ may be represented by a linear combination of $n+1$ exponentially decaying functions of t as

$$S(q,t) = \sum_{j=1}^{n+1} r_j\,\mathrm{e}^{-\Gamma_j t} \tag{6}$$

with

$$\sum_{j=1}^{n+1} r_j = 1 \tag{7}$$

Here L_j and τ_j are the strength and relaxation time for the jth relaxation mode, and r_j and Γ_j are the amplitude and decay rate of the jth decay mode. It is to be noted that the jth decay mode is not in direct correspondence with the jth relaxation mode. Therefore, Γ_j's are interrelated with τ_j^{-1}'s and $(Dq^2)^{-1}$ in somewhat involved way as shown below, and the relationship among r_j's and L_j's is also involved. Equating Eq. (1) combined with Eqs. (2) and (5) to the result calculated from Eq. (3) with Eq. (6), we obtain the following relations between Γ_j and τ_j

$$\sum_{j=1}^{n+1} \Gamma_j = D_c q^2 + \sum_{j=1}^{n} \tau_j^{-1} \tag{8}$$

$$\prod_{j=1}^{n+1} \Gamma_j = Dq^2 \prod_{j=1}^{n} \tau_j^{-1} \tag{9}$$

$$\sum_{j=1}^{n+1}\sum_{k=1}^{j-1} \Gamma_j\Gamma_k = \left[\sum_{j=1}^{n}\tau_j^{-1} + L_\pi^{-1}\sum_{j=1}^{n}L_j\sum_{k=1(k\neq j)}^{n}\tau_k^{-1}\right]Dq^2 + \sum_{j=1}^{n}\sum_{k=1}^{j-1}\tau_j^{-1}\tau_k^{-1} \tag{10}$$

$$\sum_{j=1}^{n+1}\prod_{k=1(k\neq j)}^{n+1}\Gamma_k = \left[\sum_{j=1}^{n}\prod_{k=1(k\neq j)}^{n}\tau_k^{-1} + L_\pi^{-1}\sum_{j=1}^{n}L_j\prod_{k=1(k\neq j)}^{n}\tau_k^{-1}\right]Dq^2 + \prod_{j=1}^{n}\tau_j^{-1} \tag{11}$$

where D_c is the cooperative diffusion coefficient given by

$$D_c \equiv D + \frac{(1-\phi)L_0}{c\zeta} \tag{12}$$

with L_0 the instantaneous longitudinal modulus (on the DLS time scale) defined by

$$L_0 \equiv \sum_{j=1}^{n} L_i \tag{13}$$

and L_π the osmotic compressibility (or modulus) defined by

$$L_\pi \equiv c\left(\frac{\partial\pi}{\partial c}\right)_{T,p} \tag{14}$$

The quantity K_1 defined by

$$K_1 \equiv \left[-\frac{\partial \ln S(q,t)}{\partial t} \right]_{t\to 0} \tag{15}$$

is called the first cumulant. We find for this quantity

$$K_1 = \sum_{j=1}^{n+1} r_j \Gamma_j \tag{16a}$$

$$K_1 = Dq^2 \tag{16b}$$

Eq. (16b) is derived from comparison of the coefficients of $(i\omega)^{n-1}$ in the numerators of Eq. (1) and of the result obtained by inserting Eq. (6) into Eq. (3), with the aid of Eqs. (7), (8) and (12). It gives a means to evaluate D, provided that the limit $t \to 0$ is accessible in measuring $S(q,t)$. The set of Eqs. (8)–(14) forms the target of DLS measurements attempted in the present work. However, we note that this set cannot be solved analytically to obtain τ_j and L_j from Γ_j determined experimentally, except for the cases of small n. In the present work, we evaluate only L_0 and the maximum value of τ_j or the terminal relaxation time τ_m instead of estimating individual values of L_j and τ_j, in addition to the values of D and ζ.

3. Experimental

3.1. Materials

The PIB samples used in this work is fractions separated by fractional precipitation with benzene as a solvent and methanol as a precipitant from the commercial sample Vistanex of Enjay Chemical Co. Their weight-average molecular weight M_w was determined by static light scattering measurements in n-heptane at 25.0 °C with a Fica50 light scattering photometer. The results are summarized in Table 1 along with the values of the ratio of M_w to the number-average molecular weight M_n determined by analytical gel permeation chromatography.

Isoamyl isovalerate (IAIV) (Tokyo Kasei Kogyo Co.) used as a Θ solvent was purified by distillation under reduced pressure after dehydration with potassium carbonate. n-Heptane used as a good solvent was purified according to the standard procedure.

3.2. Dynamic light scattering

DLS measurements for the n-heptane solutions were carried out using a Brookhaven Instruments Model BI-200SM light scattering goniometer and vertically polarized incident light of 488 nm wavelength from a Spectra-Physics Model 2020 argon ion laser equipped with a Model 583 temperature-stabilized etalon for single-frequency-mode operation. The photomultiplier tube used was an EMI 9863B/350, and the output was processed by a Brookhaven Instruments Model BI2030AT autocorrelator with 264 channels. On the other hand, the measurements for the IAIV solutions were made by the use of a ALV DLS/SLS-5000/E light scattering photogoniometer and correlator system with vertically polarized incident light of 632.8 nm wavelength from a Uniphase Model 1145P He–Ne gas laser. The normalized autocorrelation function $g^{(2)}(t)$ of the scattered light intensity $I(t)$, i.e.

$$g^{(2)}(t) = \langle I(0)I(t)\rangle / \langle I(0)\rangle^2 \tag{17}$$

was measured at scattering angles θ ranging from 30 to 150°.

When the field correlation function $g^{(1)}(t)$, which is essentially the same quantity as $S(q,t)$ given in Section 2, is represented by

$$g^{(1)}(t) = \sum_i r_i \, \mathrm{e}^{-\Gamma_i t} \tag{18}$$

in agreement with Eq. (6), the experimental estimator $g^{(2)}(t;\Delta t)$ for $g^{(2)}(t)$ is given by [19]

$$g^{(2)}(t;\Delta t) = 1 + f \sum_i \sum_j \frac{\sinh^2(\gamma_i+\gamma_j)}{(\gamma_i+\gamma_j)^2} r_i r_j \, \mathrm{e}^{-(\Gamma_i+\Gamma_j)t} \tag{19}$$

with

$$\gamma_i \equiv \frac{\Gamma_i \Delta t}{2}, \qquad \gamma_j \equiv \frac{\Gamma_j \Delta t}{2}; \quad t = k\Delta t \; (k = 1, 2, \ldots, 264)$$

Here, Δt is the sampling interval and f the coherence factor fixed by the optical system. Since $\sinh^2(\gamma_i+\gamma_j)/(\gamma_i+\gamma_j)^2 \simeq 1$ for appropriate values of Δt, Eq. (19) is replaced by

$$g^{(2)}(t;\Delta t) = g^{(2)}(t) = 1 + f|g^{(1)}(t)|^2 \tag{20}$$

For the case of the Brookhaven instruments, we obtained $g^{(2)}(t;\Delta t)$ for 2 to 3 different Δt and confirmed that the results were independent of the chosen Δt. We note that this procedure is not necessary for the ALV instrument.

For data analysis, we first evaluated $f^{1/2}$ and the first cumulant K_1 from the ordinate intercept and the slope of the straight line fitted to the initial linear part of the experimental $(1/2)\ln[g^{(2)}(t) - 1]$ vs. t plot near $t \simeq 0$. Then, we employed the 'procedure X', [20] to estimate r_j and Γ_j, with the main purpose of evaluating the maximum relaxation time τ_m and the instantaneous modulus L_0 as stated above. The procedure X is a familiar technique which was originally devised to determine the discrete relaxation spectrum $H(\tau)$ from the observed relaxation modulus $G(t)$. It is known that calculation of $G(t)$ with $H(\tau)$ obtained by this technique affords good approximation to the observed

Table 1
Values of M_w and M_w/M_n for polyisobutylene samples

Sample	$10^{-4}\,M_w$	M_w/M_n
PIB116	116	1.19
PIB209	209	1.23
PIB459	459	1.26

$G(t)$. In the present case, the procedure X separates the DLS decay modes from slower to faster decay rate in stepwise fashion. In practice, a plot of $(1/2)\ln[g^{(2)}(t)-1]$ vs. t gives a straight line for $t > \Gamma_1^{-1}$. Here, the subscript number is chosen so that $\Gamma_1 < \Gamma_2 < \Gamma_3 < \cdots$ without loss of generality. From the slope and the ordinate intercept of the straight line, we may determine Γ_1 and $f^{1/2}r_1$, respectively. In the next step, a plot of $(1/2)\ln\{[g^{(2)}(t)-1] - f^{1/2}r_1\exp(-\Gamma_1 t)\}$ vs. t again gives a straight line for $t > \Gamma_2^{-1}$, if Γ_2^{-1} is reasonably separated from Γ_1^{-1} and Γ_3^{-1}. The straight line allows us to determine Γ_2 and $f^{1/2}r_2$ from its slope and the ordinate intercept, respectively. The process can be repeated to find Γ_3, $f^{1/2}r_3$, and so on. As to the procedure X, some comments may be in order. First, since the decay modes closely distributed on the time axis cannot be successfully separated, the values of Γ_j and $f^{1/2}r_j$ ($j = 1, 2, 3, \ldots$) determined by the above process should be taken as some averages at appropriately separated time intervals. Second, when the processes are repeated many times, the resulting values of Γ_j and $f^{1/2}r_j$ with large j unavoidably suffer from cumulative errors and hence become less reliable. Therefore, in the present analysis, we evaluated the largest Γ_j and the corresponding $f^{1/2}r_j$ with the aid of Eqs. (7) and (16a) (or $f^{1/2}\sum_{j=1}^{n+1} r_j = f^{1/2}$) by using the values of $f^{1/2}$ and K_1 obtained above along with the results already determined for the slower decay modes.

One may argue that $[g^{(2)}(t)-1]^{1/2}$ data are more conveniently analyzed with a computer program [21,22] such as *contin* or *maxent* to determine the distribution function $r(\Gamma)$ defined by

$$[g^{(2)}(t)-1]^{1/2} = f^{1/2}\int_0^\infty r(\Gamma)\exp(-\Gamma t)\,\mathrm{d}\Gamma \tag{21}$$

However, as far as we are aware, no method to extract information about $L(t)$ from $r(\Gamma)$ is as yet established. This is the reason why we have employed the procedure X to determine discrete Γ_j and r_j in the present study.

DLS measurements were made on three PIB samples in the range of the polymer mass concentration c where polymer chains are moderately or highly entangled. Note that the value of the critical molecular weight M_c for the onset of entanglements is estimated as 1.70×10^4 for bulk PIB [23]. The value of $cM_w/(\rho^0 M_c)$, which is a measure of the existence of entanglement ranges from 2.6 to 23 for the *n*-heptane solutions and from 1.0 to 6.6 for the IAIV solutions. Here, ρ^0 is the density of bulk PIB. The measuring temperature was fixed at 25.0 °C (Θ temperature for PIB–IAIV) for all solutions. To prepare the test solution, a dilute solution of the PIB sample in cyclohexane was filtered into an optically cleaned light scattering cell with a Teflon membrane of 0.45 μm pore size. The solution was freeze-dried after the cell was covered with a Teflon membrane of the same pore size. Then, an appropriate amount of filtered solvent IAIV or *n*-heptane was poured into the cell. After the cell was tightly sealed, the solution was made homogeneous keeping the cell for 10–14 days at ca. 50 °C for IAIV and at room temperature for *n*-heptane. The polymer mass concentration c was calculated from the weight fraction and the solution density ρ, using the published relations [24,25]:

$$\rho = 0.85066 + 0.0737c \qquad (\text{PIB/IAIV}, 25.0\ ^\circ\text{C}) \tag{22}$$

$$\rho = 0.67961 + 0.237c + 0.11c^2 \qquad (\text{PIB}/n\text{-heptane}, 25.0\ ^\circ\text{C}) \tag{23}$$

4. Results

4.1. Autocorrelation function

Fig. 1 shows salient features of $g^{(2)}(t)$ for entangled PIB solutions. By virtue of Eq. (20), these data may be viewed as representing the behavior of $f^{1/2}g^{(1)}(t)$ and thus $S(q,t)$ reduced by a constant factor. Fig. 1(A) depicts angular dependence of the double-logarithmic plot of $[g^{(2)}(t)-1]^{1/2}$ against t for PIB116 in *n*-heptane at $c = 0.0652$ g/cm^3. It is seen that the decay curve at fixed scattering angle θ is roughly divided into two modes, i.e. the fast and slow modes. The decay rate of the fast mode becomes larger as θ increases, while that of the slow mode is approximately independent of θ. These results suggest that the former is mainly due to diffusion process and the latter mainly due to viscoelastic relaxation.

Fig. 1(B) shows molecular weight dependence of $(1/2)\log[g^{(2)}(t)-1]$ vs. $\log t$ plot for PIB solutions in *n*-heptane at $c = 0.066$ and 0.02 g/cm^3 and at $\theta = 120°$. It is seen that the data points obtained with different sampling intervals Δt are smoothly connected with each other, although close examination reveals slight discontinuity. Such small discrepancies are ignored in this work. At each fixed c, the fast mode is substantially independent of polymer molecular weight M_w, indicating that the decay rate in this time region is governed by local friction between polymer segments and solvent molecules. On the other hand, the slow mode extends to longer times as M_w becomes greater. The results are in line with the well known fact that the longest viscoelastic relaxation time τ_m becomes larger with increasing M_w.

In Fig. 1(C) are shown the results for PIB116 in IAIV at Θ with $c = 0.0528$ g/cm^3 and at θ ranging from 60 to 120 °. We note that the data points at $\theta = 120$ and 150 ° are almost completely overlapped over the entire range of t and the wildly scattered data in the terminal region is due to the presence of dust particles which we failed to remove. In comparison with the data for the same PIB sample in the good solvent shown in Fig. 1(A), we find that the slow mode contributes to $g^{(2)}(t)$ to a greater extent at Θ and thus the slow and fast modes are not clearly separated from each other in Fig. 1(C). Recently, similar results are obtained for

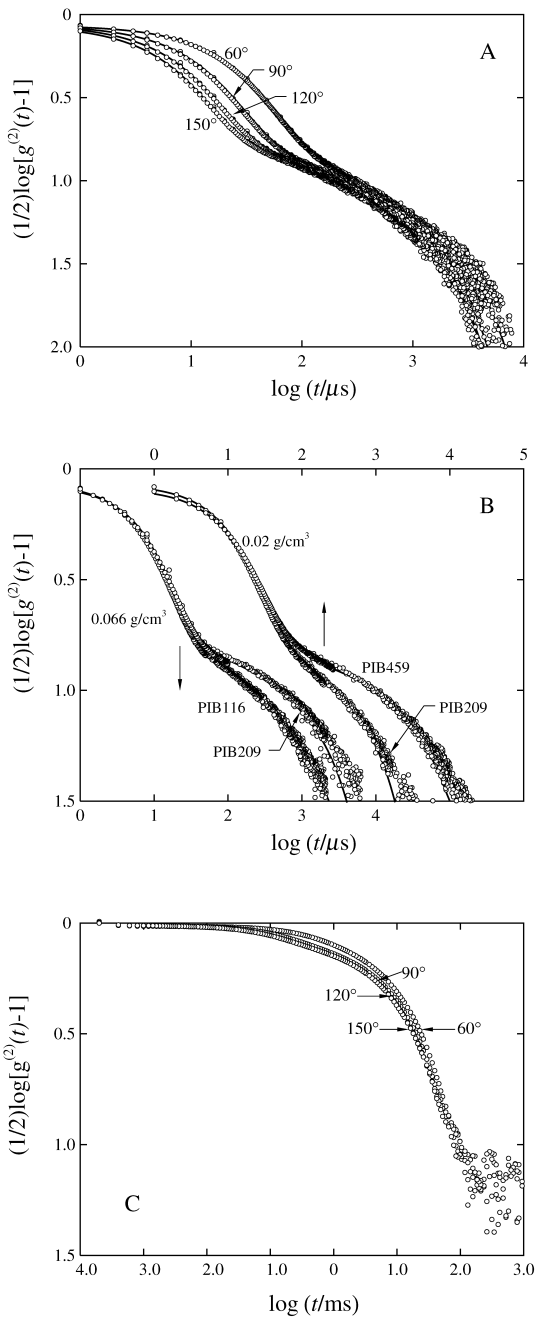

Fig. 1. Double-logarithmic plots of $[g^{(2)}(t) - 1]^{1/2}$ against t for PIB116 in n-heptane at $c = 0.0652$ g/cm^3 and at the indicated values of θ (A), for PIB116 and PIB209 at $c = 0.066$ g/cm^3 and for PIB209 and PIB459 at $c = 0.02$ g/cm^3 in n-heptane at $\theta = 120°$ (B), and for PIB116 in IAIV at $c = 0.0528$ g/cm^3 and at the indicated values of θ (C). The solid curves in (A) and (B) represent the calculated values (see text).

entangled PIB solutions near the phase separation temperature by Nicoli and Brown [17].

4.2. Data analysis

Figs. 2 and 3 present the examples of the plots on the basis of Eqs. (8)–(10), (16a), and (16b) for PIB116 solutions in n-heptane. Here the $g^{(2)}(t)$ data for these

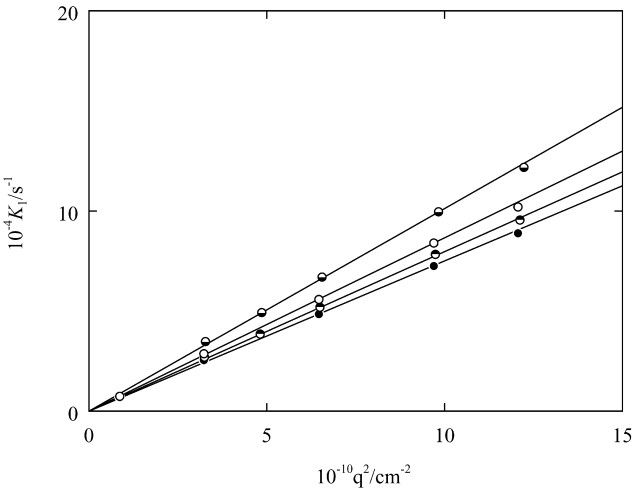

Fig. 2. Plots of K_1 against q^2 for PIB116 in n-heptane at various c: c is 0.110, 0.0714, 0.0652, and 0.0427 g/cm^3 from top to bottom, respectively.

solutions were successfully separated into a series of exponential functions by the procedure X as stated in Section 3, on the assumption that they were approximated by summation of four exponential terms, i.e. $n = 3$ in Eq. (6) or (18). The solid curves in Fig. 1(A) and (B), calculated from Eqs. (18) and (20) with the values of r_j and Γ_j thus determined, show good fit to the data points.

Fig. 2 shows the examples of the first cumulant K_1 plotted against q^2, where $q = 4\pi n_0 \sin(\theta/2)/\lambda_0$ with n_0 the refractive index of the solvent and λ_0 the wavelength of the incident light in vacuum. As required by Eq. (16b), the data points at fixed c follow a straight line passing through the origin. Thus, we have been able to determine accurately the value of D from its slope.

Fig. 3(A) gives the plots corresponding to Eq. (8). It is seen that the data points for each solution fall on a straight line as expected from Eq. (8). From its slope and ordinate intercept, we have obtained the values of D_c and the sum of three reciprocal relaxation times, i.e. $\sum_{j=1}^{3} \tau_j^{-1}$, respectively. In Fig. 3(B) and (C) are given the plots corresponding to Eqs. (9) and (10), respectively. In the former, we find that the data set at fixed c follows a straight line passing through the origin as expected from Eq. (9), from whose slope we have evaluated the product of D and three reciprocal relaxation times, i.e. $D\prod_{j=1}^{3} \tau_j^{-1}$. Then, we have calculated the value of $\prod_{j=1}^{3} \tau_j^{-1}$ by dividing it by D evaluated from K_1 above. In Fig. 3(C), the data points at fixed c fall on a straight line as predicted by Eq. (8), thereby allowing us evaluations of the coefficient of q^2 and the constant term on the right hand side of Eq. (8) from its slope and ordinate intercept, respectively.

From these analyses, we have obtained the values of D, D_c, and τ_m. Here, the minimum value of τ_j^{-1} calculated from the results for $\sum_{j=1}^{3} \tau_j^{-1}$, $\prod_{j=1}^{3} \tau_j^{-1}$, and $\sum_{j=1}^{3} \sum_{k=1}^{j-1} \tau_j^{-1}\tau_k^{-1}$ has been assigned to τ_m^{-1}. The data for $g^{(2)}(t)$ obtained for all the solutions examined have been analyzed in a similar manner. The values of D and τ_m thus determined are listed

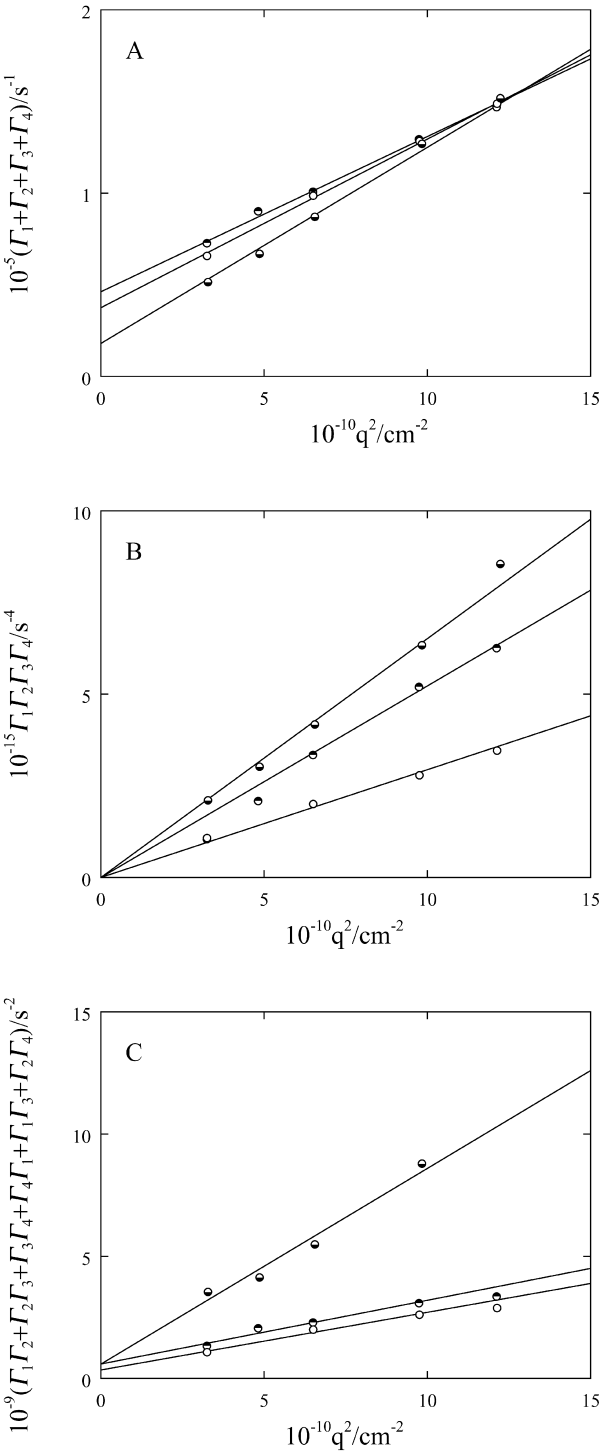

Fig. 3. Plots of $\sum_{j=1}^{4}\Gamma_j$ (A), $\prod_{j=1}^{4}\Gamma_j$ (B), and $\sum_{j=1}^{4}\sum_{k=1}^{j-1}\Gamma_j\Gamma_k$ (C) against q^2 for PIB116 in *n*-heptane at various *c*. The symbols have the same meaning as those in Fig. 2.

in Table 2 along with those of ζ and L_0 calculated below. We note that the values of L_0 and τ_m do not depend on the mode number n chosen in the procedure X, so long as $g^{(2)}(t)$ calculated from Eqs. (18) and (20) with the values of r_i and Γ_i $(i = 1, 2, \ldots, n)$ coincides with the observed results as found in Fig. 1(A) and (B).

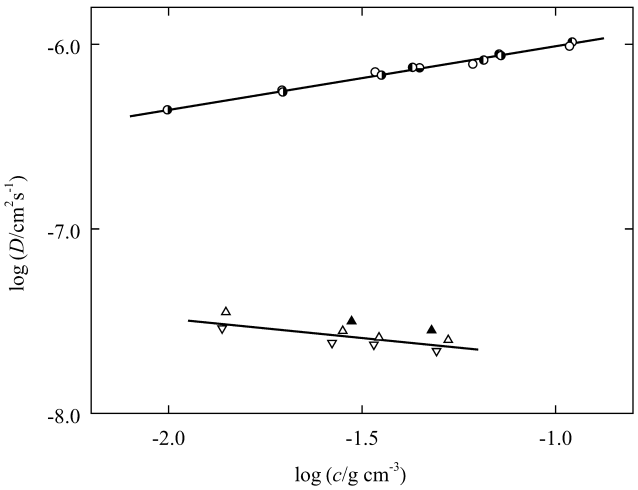

Fig. 4. Double-logarithmic plots of D against c for PIB in *n*-heptane (circles) and in IAIV (Θ) (triangles) for various M_w : right-half-filled circles, PIB459; unfilled circles, PIB209; left-half-filled circles, PIB116; bottom-half-filled circle, $M_w = 8.15 \times 10^5$ [11]; unfilled triangles down, PIB209; unfilled triangles up, PIB116; filled triangles, $M_w = 8.15 \times 10^5$ [11].

5. Discussion

5.1. Translational diffusion and friction coefficients

Concentration dependence of D for PIB in *n*-heptane at 25.0 °C (circles) and in IAIV at 25.0 °C (Θ) (triangles) is indicated in Fig. 4, where the previous data by Einaga and Karube [11] are also included. It is found that the dependence is markedly different between the two systems depending upon the solvent quality. For the case of the *n*-heptane solutions, D gradually increases with increasing c and is independent of M_w. On the other hand, D for the IAIV solutions gradually decreases with increasing c and D at fixed c slightly decreases with increasing M_w.

D in Eq. (12) is related to the friction coefficient ζ by

$$D = \frac{(1 - vc)L_\pi}{c\zeta} \tag{24}$$

where v is the partial specific volume of the polymer component. This relation is valid for the solute diffusion relative to the solvent component, or in other words, for the solute flow relative to the solvent-fixed frame. On the other hand, for DLS experiments where the solute diffusion relative to the laboratory-fixed frame is observed, the following relation should be employed instead of Eq. (24) [26,27]:

$$D = \frac{(1 - vc)^2 L_\pi}{c\zeta} \tag{25}$$

With this equation, we calculated the values of ζ corresponding to D, in which we used the L_π values calculated from

$$L_\pi = cRT\left(M_w^{-1} + 2A_2c + 3A_3c^2\right) \tag{26}$$

Table 2
Results of DLS measurements on polyisobutylene in *n*-heptane at 25.0 °C and in IAIV at 25.0 °C (Θ)

Sample	c (g/cm^3)	D (cm^2/s)	ζ (dyne s/cm/g)	L_0 (dyne/cm^2)	τ_m (s)
n-heptane at 25.0 °C					
PIB116	0.0427	7.51×10^{-7}	3.80×10^{12}	1.10×10^{4}	8.58×10^{-4}
	0.0652	8.22×10^{-7}	7.36×10^{12}	2.56×10^{4}	5.96×10^{-3}
	0.0714	8.86×10^{-7}	7.86×10^{12}	2.90×10^{4}	1.09×10^{-2}
	0.110	1.03×10^{-6}	1.42×10^{13}	7.09×10^{4}	2.94×10^{-2}
PIB209	0.0196	5.65×10^{-7}	1.69×10^{12}	2.53×10^{3}	4.86×10^{-4}
	0.0342	7.09×10^{-7}	3.60×10^{12}	7.44×10^{3}	2.30×10^{-3}
	0.0611	7.82×10^{-7}	9.27×10^{12}	2.44×10^{4}	1.89×10^{-2}
	0.109	9.78×10^{-7}	2.03×10^{13}	9.16×10^{4}	2.27×10^{-1}
PIB459	0.00993	4.42×10^{-7}	9.11×10^{11}	5.83×10^{2}	9.44×10^{-4}
	0.0197	5.52×10^{-7}	2.50×10^{12}	2.38×10^{3}	1.20×10^{-2}
	0.0355	6.81×10^{-7}	6.02×10^{12}	6.81×10^{3}	1.22×10^{-1}
	0.0722	8.70×10^{-7}	1.74×10^{13}	2.89×10^{4}	2.00×10^{0}
IAIV at 25.0 °C (Θ)					
PIB116	0.0141	3.54×10^{-8}	6.87×10^{11}	3.58×10^{2}	1.72×10^{-3}
	0.0282	2.63×10^{-8}	1.71×10^{12}	2.48×10^{3}	1.50×10^{-2}
	0.0350	2.58×10^{-8}	2.34×10^{12}	4.71×10^{3}	7.33×10^{-2}
	0.0528	2.50×10^{-8}	4.69×10^{12}	1.70×10^{4}	3.05×10^{-1}
PIB209	0.0137	2.89×10^{-8}	5.13×10^{11}	2.55×10^{2}	2.55×10^{-2}
	0.0264	2.41×10^{-8}	1.34×10^{12}	9.02×10^{2}	3.51×10^{-1}
	0.0339	2.36×10^{-8}	2.07×10^{12}	4.57×10^{3}	1.45×10^{0}
	0.0492	2.18×10^{-8}	4.38×10^{12}	1.74×10^{4}	2.86×10^{0}

where R is the gas constant, T the absolute temperature and A_2 and A_3 are the second and third virial coefficients, respectively. We note that the use of Eq. (26) is somewhat rough approximation at high concentrations. For the *n*-heptane solutions, we used the A_2 and A_3 values evaluated for each PIB sample by extrapolating the Akasaka et al.'s data [25] up to the corresponding M_w value and $v = 1.046\ \mathrm{cm^3/g}$ calculated from Eq. (23). For the IAIV solutions, we used $A_2 = -0.8\times10^{-5}\ \mathrm{mol\ cm^3/g^2}$ and $A_3 = 6.3\times10^{-4}\ \mathrm{mol\ cm^6/g^3}$ for a PIB sample with $M_w = 8.72\times10^5$ [24], and $v = 0.931\ \mathrm{cm^3/g}$ calculated from Eq. (22).

The results for ζ thus calculated are summarized in Table 2 and double-logarithmically plotted against c in Fig. 5. It is seen that ζ increases with increasing c following a straight line with slope ca. 1.6, indicating a power-law behavior. The value of the slope, i.e. the exponent of c, is independent of M_w and solvent quality. This result implies that marked difference in the c dependence of D between the good and Θ solvent systems found in Fig. 4 arises from the difference in the driving force for the mutual diffusion: the osmotic compressibility L_π increases much more rapidly with c in the good solvent system than the Θ solvent.

5.2. Rubbery plateau modulus

The values of the instantaneous longitudinal modulus L_0 have been determined by Eq. (12) from those of D_c in combination with the results for D and ζ given above. They are summarized in Table 2 together with the values of D, ζ, and τ_m, and double-logarithmically plotted against c in Fig. 6, where the previous data by Einaga and Karube [11] are also included. According to the theoretical analysis by Chen and Berry [6], L_0 may be correlated to the rubbery plateau modulus G_N by

$$L_0 = (4/3)G_N \tag{27}$$

Thus for reference, Fig. 6 includes the value of $(4/3)G_N$ determined for bulk PIB [23,28] (filled circle) by mechanical

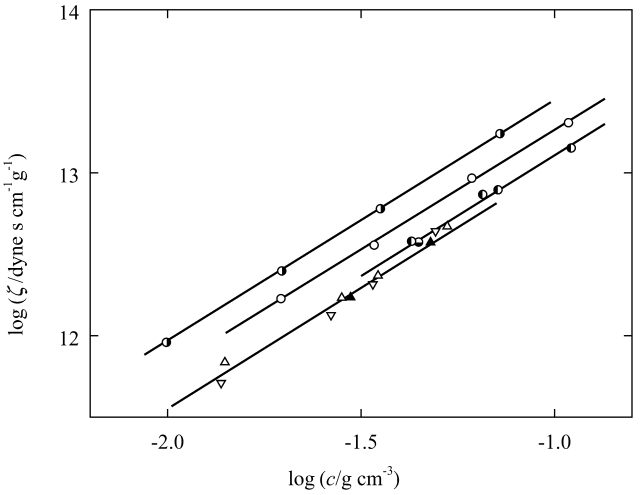

Fig. 5. Double-logarithmic plots of ζ against c for PIB in *n*-heptane (circles) and in IAIV (Θ) (triangles). The symbols have the same meaning as those in Fig. 4.

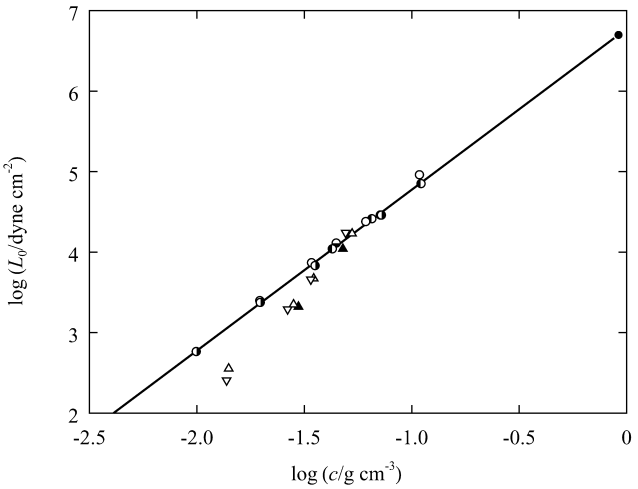

Fig. 6. Double-logarithmic plots of L_0 against c for PIB in n-heptane (circles) and in IAIV (Θ) (triangles). Filled circle indicates the value for bulk PIB. The other symbols have the same meaning as those in Fig. 4. The solid line represents the values calculated by Eq. (28).

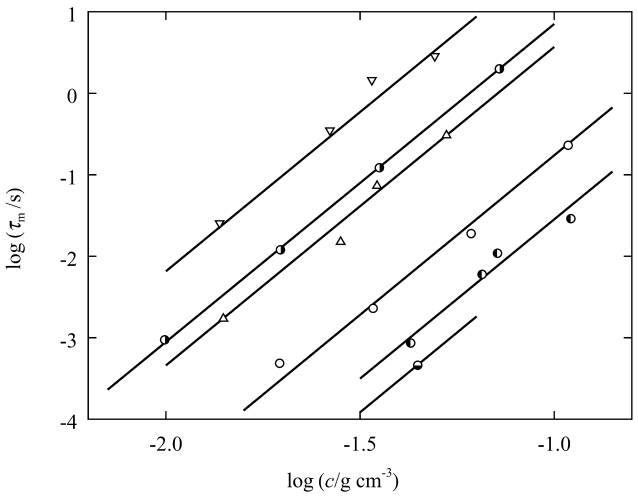

Fig. 7. Double-logarithmic plots of τ_m against c for PIB in n-heptane (circles) and in IAIV (Θ) (triangles). The symbols have the same meaning as those in Fig. 4.

or rheological measurements. The straight line in this figure represents the familiar relation [6,29]

$$G_N = G_N^0\left(\frac{c}{\rho^0}\right)^2 \tag{28}$$

where G_N^0 is the rubbery plateau modulus. The data points for the n-heptane solutions (circles) closely follow this line irrespective of the M_w value, thereby obeying Eq. (28). We note that G_N^0 is known to be independent of M_w. On the other hand, while the data points for the IAIV solutions (triangles) at high concentrations also fall on the straight line, they deviate progressively downward from the line as c is decreased. The behavior suggests that the entanglement density or the number of entanglements per unit volume at low c decreases as the solvent quality decreases toward the Θ state. We have recently found the similar behavior of L_0 for moderately concentrated solutions of atactic polystyrene in good and Θ solvents [30].

It is often discussed [6,31] that Eq. (28) holds only at Θ state but for the good solvent systems, the exponent becomes somewhat larger than 2, reflecting the excluded-volume effect on the entanglement spacings, i.e. on the polymer chain between two adjacent entanglement points. The present results are not in line with this picture.

5.3. Terminal relaxation time

Fig. 7 shows double-logarithmic plots of τ_m against c for PIB in n-heptane at 25.0 °C (circles) and in IAIV at Θ (triangles). In the region of c observed, the τ_m vs. c relation is found to obey a power-law behavior with the same exponent ca. 4 irrespective of M_w and solvent quality. Interpretations of this result or the value of the exponent are not easy at present, since the relationship between τ_m and c depends not only on the structure factor $F(c,M)$ which represents the entanglement density but on the c dependence of the segmental friction coefficient $\zeta_s(c)$ [6,18]. The c dependence of τ_m may be represented as

$$\tau_m = \zeta_s(c)F(c,M) \tag{29}$$

with

$$F(c,M) \propto \frac{(cM)^{3.4}}{G_N(c)} \tag{30}$$

If we assume that $\zeta_s(c)$ depends on c in the same fashion as ζ shown in Fig. 5, Eqs. (29) and (30) in combination with the results in Fig. 6 predict τ_m as a function of c as

$$\tau_m \propto c^3 \qquad \text{(for } n\text{-heptane solutions)} \tag{31a}$$

$$\tau_m \propto c^2 \qquad \text{(for IAIV solutions)} \tag{31b}$$

The observed exponential (found in Fig. 7) is larger than the prediction given in Eqs. (31a) and (31b). This discrepancy may suggest that the c dependence is different for ζ_s and ζ.

In Fig. 8, τ_m at fixed c for n-heptane solutions (unfilled circles) and for the IAIV solutions (filled circles) is double-logarithmically plotted against M_w. Here, the τ_m values were evaluated by interpolating the data in Fig. 7 to $c = 0.04$ g/cm^3. The data points for each system roughly follow a straight line with slope 3.4. This result is in good coincidence with the familiar relation $\tau_m \propto M_w^{3.4}$ found for the entangled polymer systems by rheological measurements [18].

6. Concluding remarks

The normalized intensity autocorrelation function $g^{(2)}(t)$ has been determined by DLS measurements for moderately concentrated PIB solutions in n-heptane at 25.0 °C and in IAIV at Θ. The novel method for the analysis of $g^{(2)}(t)$ proposed by us [11] on the basis of the recent phenomenological theory [7,8,10,11] has been applied to the obtained

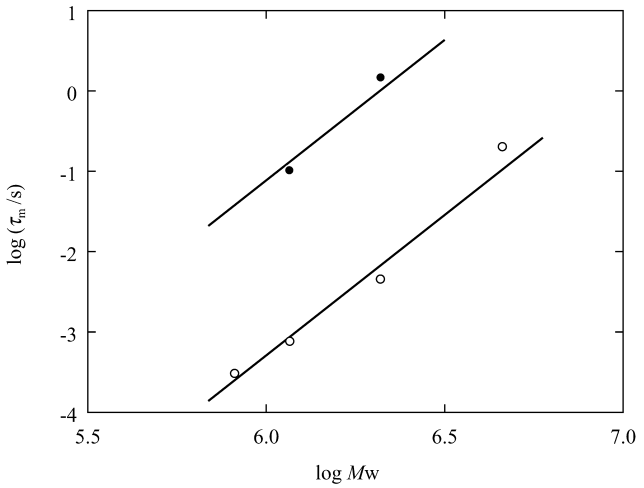

Fig. 8. Double-logarithmic plots of τ_m against M_w for PIB in *n*-heptane (unfilled circles) and in IAIV (Θ) (filled circles) at $c = 0.04\ g/cm^3$. The solid lines are drawn with slope 3.4.

data. The results have shown that in addition to the frictional properties such as the mutual diffusion coefficient D and friction coefficient ζ, the viscoelastic properties such as the longitudinal rubbery plateau modulus L_0 and the terminal relaxation time τ_m are successfully determined for the polymer solutions under the rigorously controlled solvent and temperature condition to which conventional mechanical or rheological measurements are hardly accessible.

The obtained viscoelastic properties for the above solutions are in line with the results accumulated so far from the rheological measurements for bulk polymers and highly concentrated polymer solutions. For example,

1. the rubbery plateau modulus L_0 for the *n*-heptane solutions increases with increasing c in proportion to c^2 and
2. the terminal relaxation time τ_m for both systems is proportional to $M_w^{3.4}$.

However, rather new type of c dependence of L_0 has been found for the IAIV solutions at Θ.

Although the procedure X used in the present study is a powerful method to determine the diffusive and viscoelastic properties of entangled polymer solutions, it is somewhat tedious and delicate operation. It is, thus, highly desirable to obtain the longitudinal relaxation modulus $L(t)$ more directly from $g^{(2)}(t)$ or $S(q,t)$. In so doing, we need a mathematical relation between $L(t)$ and $S(q,t)$ which may be obtained by solving Eq. (1) in combination with Eqs. (2) and (3), and a experimental procedure based on it.

Acknowledgments

This research was supported in part by a Grant-in-Aid (11450368) from the ministry of Education, Science, and Culture, Japan.

References

[1] Lustig SR, Caruthers JM, Peppas NA. Chem Engng Sci 1992;47:3037.
[2] Billovits GF, Durning CJ. Macromolecules 1994;27:7630.
[3] Herman MF, Edwards SF. Macromolecules 1990;23:3662.
[4] Brochard F. J Phys (Paris) 1983;44:39.
[5] Adam M, Delsanti M. Macromolecules 1985;18:1760.
[6] Chen S-J, Berry GC. Polymer 1990;31:793.
[7] Doi M, Onuki A. J Phys II (Paris) 1992;2:1631.
[8] Onuki A. J Non-Cryst Solids 1994;172–174:1151.
[9] Berry GC. Adv Polym Sci 1994;114:233.
[10] Einaga Y, Fujita H. Polymer 1999;40:565.
[11] Einaga Y, Karube D. Polymer 1998;40:157.
[12] Brown W, Nicolai T. Colloid Polym Sci 1990;268:977. references cited therein.
[13] Koike A, Nemoto N, Inoue T, Osaki K. Macromolecules 1995;28:2339.
[14] Nemoto N, Koike A, Osaki K. Macromolecules 1996;29:1445.
[15] Jian T, Vlassopoulos D, Fytas G, Pakula T, Brown W. Colloid Polym Sci 1996;274:1033.
[16] Štěpánek P, Brown W. Macromolecules 1998;31:1889.
[17] Nicoli T, Brown W. Macromolecules 1999;32:2646.
[18] Ferry JD. Viscoelastic properties of polymers, 3rd ed. New York: Wiley; 1980.
[19] Pike ER, Jakeman E. Adv Quantum Electron 1974;2:1.
[20] Tobolsky AV. Properties and structure of polymers. New York: Wiley; 1960.
[21] Provencher SW. Makromol Chem 1979;180:201.
[22] Livesey AK, Licinio P, Delaye M. J Chem Phys 1986;84:5102.
[23] Fetters LJ, Lohse DJ, Milner ST, Graessley WW. Macromolecules 1999;32:6847.
[24] Akasaka K, Nakamura Y, Norisuye T, Teramoto A. Polym J 1994;26:363.
[25] Akasaka K, Nakamura Y, Norisuye T, Teramoto A. Polym J 1994;26:1387.
[26] Berne BJ, Pecora R. Dynamic light scattering. New York: Wiley; 1976. Chapter 13.
[27] Štěpánek P, Brown W, Hvidt S. Macromolecules 1996;29:8888.
[28] Fetters LJ, Lohse DJ, Richter D, Witten TA, Zirkel A. Macromolecules 1994;27:4639.
[29] Einaga Y, Osaki K, Kurata M, Tamura M. Macromolecules 1972;5:635.
[30] Einaga Y, Fujisawa T. Polymer, in press.
[31] Adam M, Fargo B, Schleger P, Raspaud E, Lairez D. Macromolecules 1998;31:9213.